Eur. Phys. J. D **30**, 353–362 (2004)
DOI: 10.1140/epjd/e2004-00108-1

THE EUROPEAN PHYSICAL JOURNAL D

Charged cores in ionized ^{4}He clusters II: Ab initio calculations for the $He_2^+ + He$ system and Many-Body fitting of the computed points

E. Scifoni[1,2], G. Dellepiane[1], and F.A. Gianturco[2,a]

[1] Department of Chemistry and Industrial Chemistry, University of Genoa, via Dodecaneso 31, 16146 Genoa, Italy
[2] Department of Chemistry and INFM, University of Rome "La Sapienza", Piazzale A. Moro 5, 00185 Rome, Italy

Received 10 March 2004 / Received in final form 15 June 2004
Published online 24 August 2004 –

Abstract. Experimental and theoretical studies in large, ionized helium clusters have suggested the presence of structures in which a diatomic (and occasionally triatomic) charged molecular core is surrounded by nearly neutral atoms which are bound to it by weaker forces. The understanding of the interactions between the He_2^+ system and one of the neutral He atoms of the cluster is therefore crucial in order to understand the microscopic dynamics of the post-ionization evolution. The first part of this work [Eur. Phys. J. D **21**, 323 (2002)] reported the Potential Energy Surface (PES) for the interaction between the He_2^+ and an He atom and described its bound states. Since dynamical calculations require a more extensive variable range of the relevant PES to be sampled, we present here a further, more detailed study in which we span a larger configurational space for the three internal coordinates of the title system. In particular, we have included a greater range of internuclear distances of the molecular ion. The resulting ab initio values have been numerically fitted via an analytic expression in terms of the three internuclear distances within the He_3^+ system. As a first step in the analysis of the dynamics we have calculated the vibrational coupling terms which involve the ionic core vibrational wave functions and the interaction of the latter molecule with the external helium atom. They reveal interesting features and properties that are here discussed.

PACS. 34.20.Mq Potential energy surfaces for collisions – 34.50.Ez Rotational and vibrational energy transfer – 36.40.Wa Charged clusters

1 Introduction

The peculiar environment existing in ionized He clusters is currently an intriguing research field where many fundamental questions are still open. These clusters can further act as hosts to various molecular dopants, thereby helping us to better understand solvation processes. From the fairly large amount of theoretical and experimental works carried out in the last 20 years in this field [2–12] it emerges quite clearly the specific interest on the microscopic mechanism for the localization of the charge produced by a primary ionization event. It is known, in fact, that when helium clusters are ionized by electron or photon impact, the first process is the formation of a single atomic ion somewhere in the cluster. The behaviour of the whole cluster after ionization is still under debate because of the large excess of deposited energy which has to be dissipated. The aggregate probably evolves through some metastable situation where a small ionic core is being formed [5]. The latter is made up by a restricted number of atoms that share the charge, while the remaining, almost neutral atoms are bound to it via induction and dispersion forces. The diatomic or triatomic core, when formed, is likely to be in a highly excited vibrational state from which it decays through its interactions with the surroundings atoms and leads to dissipating its excess energy via evaporation of the host cluster atoms. This picture, although only partially confirmed by the experimental observation [5], may be used to explain the large rates of evaporation of He droplets after the ionization event and the fact that the smallest fragments He_2^+/He_3^+ (with a large predominance of the first one) give rise to strong peaks in the mass spectra [5]. The former part of the present study [1] described the Potential Energy Surface (PES's) and the bound states of the $He_2^+(r)-$He system at different interatomic distances r. In the same work [1] we also calculated the vibrational levels of the He_2^+ molecular ion, obtaining for it a total of 23 bound states. In the present extension we intend to generate the relevant interaction forces to be employed for the corresponding

[a] e-mail: fa.gianturco@caspur.it

dynamical computations reported in the following paper [13]. We also provide here for the first time a global fit of the full three-dimensional Potential Energy Surface of the He_3^+ system, obtained from an extended ab initio sampling of the configurational points, while previous works produced results for more limited configurational regions [14, 15].

The possible efficiency of the vibrational relaxation step is certainly a crucial but still unknown quantity, although our earlier calculations on this very system, at ultra-low temperatures, have already found large efficiency for the simpler rotational deexcitation events [16]. The first step in our study therefore requires to evaluate the rovibration-to-translation (R,V-T) coupling potential that stems from the three-dimensional PES convoluted over asymptotic He_2^+ vibrational functions $\varphi_i(r)$ for different states of the diatomic moiety: the above procedure will be discussed in detail in Section 4.

2 The extended ab initio potential energy surface

In the earlier PES calculations [1] we used Jacobi coordinates, shown in the inset of Figure 1. For the equilibrium distance of He_2^+ we have found that the angular anisotropy was rather smooth so that the whole surface could be mapped by a fairly small angular grid of only four values of θ between 0° and 90°. In fact, when expanding the ab initio points in terms of Legendre polynomials

$$V(R,\theta) = \sum_{\lambda} V_\lambda(R) P_\lambda(\cos\theta) \qquad (1)$$

it was possible to generate quite accurately all angular configurations by recombining these coefficients and using just a few λ values ($\lambda_{max} = 6$). When one modifies the dimer interatomic distance, however, the corresponding topology of the PES experiences marked changes due to the presence, for certain orientations and distances, of non-adiabatic couplings with the upper $^2B_1$ excited state. The PES therefore shows a more complicated shape with strong angular anisotropy that requires, to be well described, a greater number of angular points. We therefore carried out new calculations with the same basis set and method as before (CCSD(T), aug-cc-pVQZ [17]), obtaining a total of 10 different angles, from 0° to 90°, for nine r values ranging from 1.0 a.u. to 8.0 a.u. and for several R values from 0.0 up to 15.0 a.u. At that R value we obtain a satisfactory merging, for any orientation, with the long range polarizability curve

$$V(R)_{(a.u.)} = -\alpha_{pol}/(2R^4), \qquad (2)$$

where $\alpha_{pol} = 1.38$ a.u.^{3} [18] is the He experimental polarizability (see also [1]). In each radial curve the ΔR spacing varied from a minimum of 0.1 a.u. up to a maximum of 0.5 a.u., depending on the angular position. The total number of directly computed points for the three-dimensional (3D) PES was about 5,000. They are available on request from the authors.

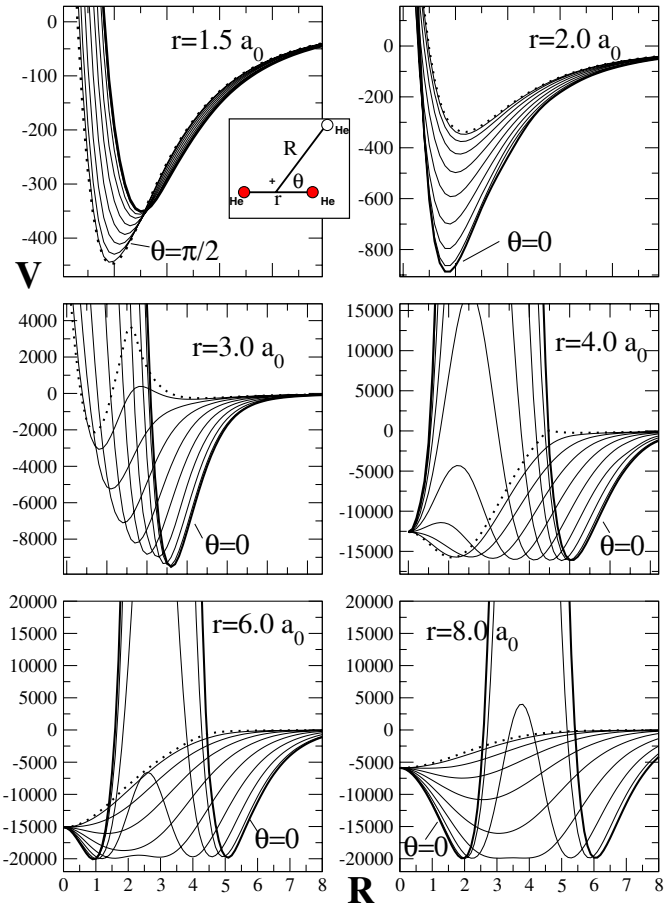

Fig. 1. He_3^+ computed 3D Potential Energy Surface reported in each panel at different angular values and for fixed r values, as a function of R, from $\theta = 0$ (bold curve) to $\pi/2$ (dotted curve). Distances are in a.u. and energies in cm^{-1}.

Some cuts of the resulting 3D PES are shown in Figure 1 at some selected values of r: in each panel r is kept fixed and the PES is reported for a set of θ values. The collinear geometry ($\theta = 0°$) is marked by a thicker line, the perpendicular one ($\theta = 90°$) with a dotted line and the curves with the deepest minima are labelled by their angular values. One sees that, excluding the case of the compressed bond ($r = 1.5\,a_0$), all other curves present their minima in the collinear geometries.When considering $r = 1.5$ (or any other geometry where the core bond is shortened), the behaviour is inverted: the minimum energy configuration is the C_{2v} geometry. One further sees that for the stretched-bond configurations all the curves representing angles different from $\theta = 0°$ become more attractive. Another important feature shown by our calculation is the appearance for $\theta \sim 90°$ of a series of cusps in the short radial range and for geometries in which the molecular bond is stretched, as, for example, in the $r = 3.0\,a_0$ (second panel on the left from the top of Fig. 1). As already discussed in our previous work [1], the cusps are due to the crossings between the ground $^2A_1$ and the first excited $^2B_1$ states in the C_{2v} geometry. This crossing is always present in the surfaces and provides an additional fragmentation

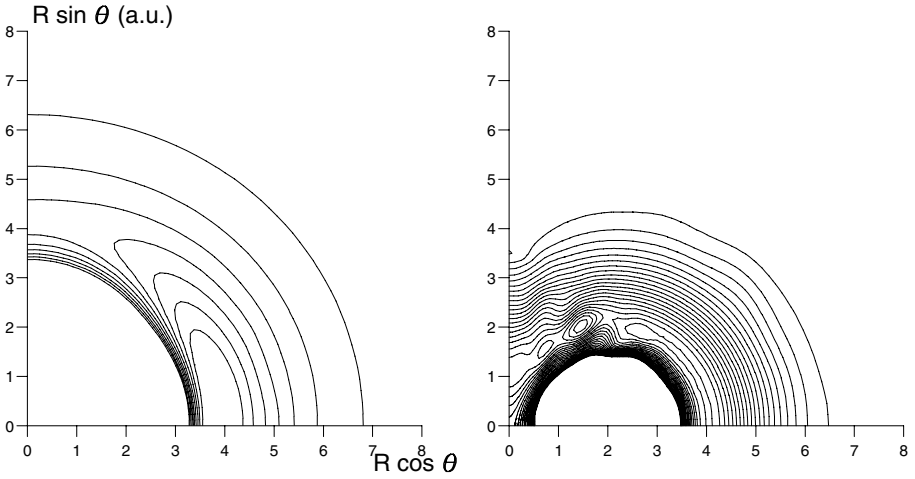

Fig. 2. He_3^+ PES contour map in Cartesian coordinates at the equilibrium r distance (left) and in a stretched molecular configuration (right, $r = 4.0$ a.u.). Equidistant contour lines are traced respectively from -100 cm^{-1} with spacing 100 cm^{-1} (left panel) and from -800 cm^{-1} with spacing 800 cm^{-1} (right panel). The oscillations shown in the right panel are due to the additional interpolation by the visualization software.

channel ($He_2 + He^+$), albeit at higher asymptotic energies. However, while for small values of r it lies in a much higher repulsive region and doesn't modify the shape of the curve in its attractive region, for larger r values the difference between the asymptotic energies of the corresponding two possible fragments, $He_2^+(r)$ and $He_2(r)$, becomes smaller thereby making the crossing to appear at lower energies.

In the right panel of the second row of Figure 1 we can see the situation at $r = 4.0\,a_0$: the shape of the surface is completely changed. The repulsive barrier for geometries near the collinear one is replaced by nuclear repulsion cusp due to the steric repulsion of two helium atoms. In these geometries the system is close to its global minimum [1] and the interaction is very strong: in the large-angle geometries there is no turning point. Further stretching of the r coordinate (two bottom panels of Fig. 1) brings the steric cusp, which survives only for a narrow angular cone around $\theta = 0°$, to larger R distances. It is worth noting here that there is also a large energy gain when we increase the r distances beyond the equilibrium value ($\sim 2\,a_0$). Indeed, the net interaction increases by one order of magnitude when going from $2\,a_0$ to $3\,a_0$.

In Figure 2 we have drawn a contour plot in cylindrical coordinates of the "rigid rotor" PES's for two values of the internuclear distance r. When comparing them, one sees how the repulsive core moves to larger radial distances, generating the marked steric cusps that we have commented on before. Less evident, but still visible on the right panel of Figure 2, is the presence of a second cusp due to the crossing of the first two electronic states at the geometries corresponding to an equilateral triangle (D_{3h}). For completeness, the angular dependence of the surface, is presented in Figure 3 for a set of selected R values and for two r distances (4.0 and $6.0\,a_0$).

An interpolation of the whole set of computed ab initio points was carried out by keeping the physical picture of the two distinct partners (He_2^+ and He) thereby using the Jacobi coordinates representation. After interpolating with cubic splines the R curves at each geometry (r, θ) within the region spanned by the ab initio points, $[0, 15\,a_0]$, and testing that this representation doesn't

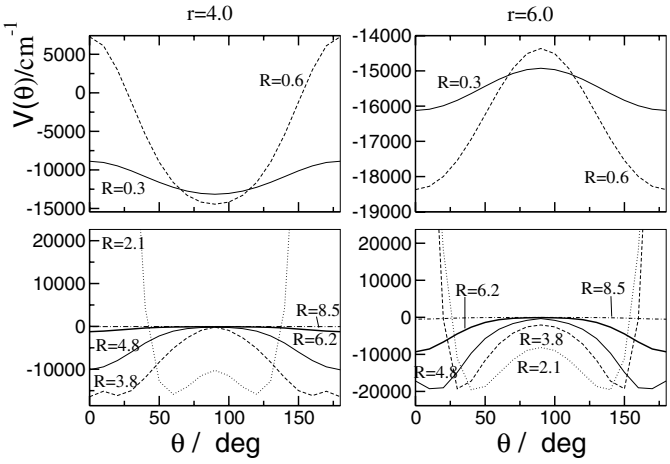

Fig. 3. Angular dependence of the PES for two of the stretched configurations of the molecular core ($r = 4$ and $6\,a_0$), shown for the short (upper panels), medium and long (lower panels) R range of values (distances in a_0).

cause spurious oscillations, the interpolated curves were merged with the spherical dipole polarizability long-range potential (Eq. (2)). In the angular variable the interpolation was performed using the multipolar expansion of equation (1), from which we obtain

$$V(r, R, \theta) = \sum_{\lambda} V_\lambda(r, R) P_\lambda(\cos\theta). \qquad (3)$$

In Figure 4 we show selected $V_\lambda(r, R)$ curves from the PES at some fixed r values and for the first eight λ values. In the first panel we can clearly see the large contributions from the spherical term ($\lambda = 0$) which persist also for stretched configurations. We further see in the other panels that the next two terms are the most anisotropic and also very important. However, when we look at the lowest panel on the right, we realize that this expansion does not satisfactorily converge. In fact, this kind of interpolation presents discontinuities in the inner regions for some of the stretched dimer configurations, as we shall further discuss below.

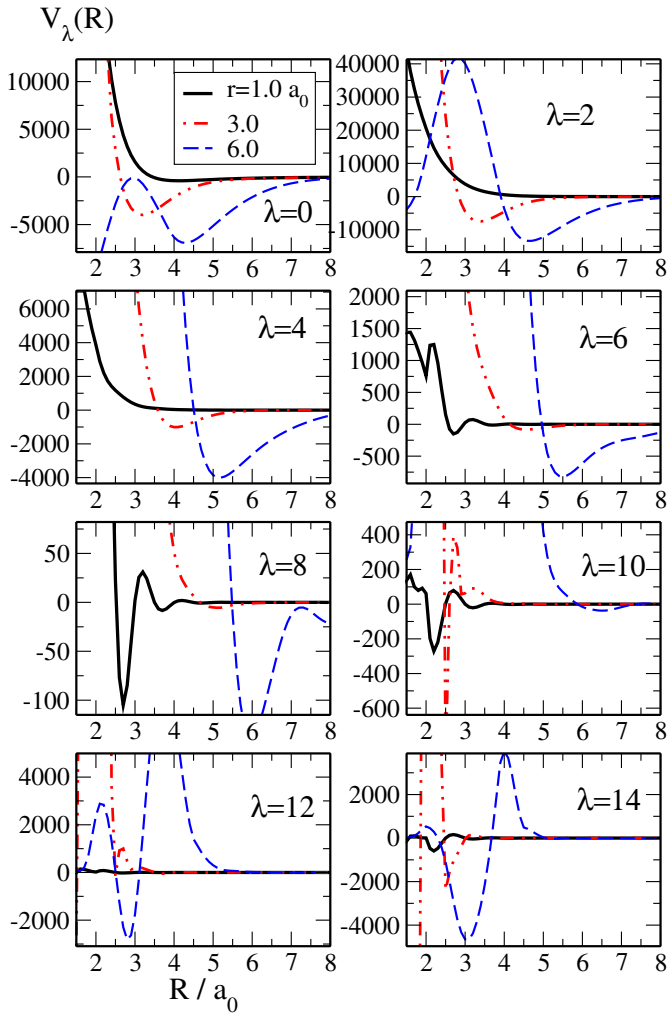

Fig. 4. Selected $V_\lambda(r, R)$ curves for the He_2^+–He PES at some fixed r values.

3 The analytic fitting procedures

In order to correctly describe this triatomic system, it is therefore more expedient to switch to internal coordinates R_1, R_2, R_3 (the distances between each of the three atoms), by simple trigonometry. In order to generate a many-body (MB) fit of the computed potential energy surface $V(R_1, R_2, R_3)$, we have followed the Aguado-Paniagua prescription [19] and isolated the three-body (3B) contribution from the two-body (2B) ones:

$$V_{ABC}(\mathbf{R}) = \sum_i^3 V_i^{(1B)} + \sum_i^3 V_i^{(2B)}(R_i) + V^{(3B)}(R_1, R_2, R_3) \tag{4}$$

where the term labeled with (1B) contains the electronic energies of the 3 isolated atoms (−7.8048784 a.u.) and the terms labeled (2B) represent the interactions between each couple of atoms. Since we are dealing with an ionic partner, we need also to take into account the specific long-range behaviour of the system. The long-range interaction is also made up of three- and two-body contributions where the charge-polarizability interaction is the leading one. It is possible to define the V^{3B} term by subtracting three, non-identical V^{2B} contributions from the total potential. Two of the diatomic interactions are taken as the charged dimer, $V_{He_2^+}(R_i)$ while the third is the neutral dimer, $V_{He_2}(R_j)$. Thus, at each configuration (R_a, R_b, R_c) the "neutral" interaction by convention is assigned to the largest among the R_i values, that is

$$V^{(3B)}(R_a, R_b, R_c) = V(R_a, R_b, R_c) - V^{(1B)} - V^{(2B)}_{He_2^+}(R_a) - V^{(2B)}_{He_2^+}(R_b) - V^{(2B)}_{He_2}(R_c), \tag{5}$$

with

$$R_c \geq R_b \geq R_a.$$

Using this definition, the 3-body interaction, does not contain any long range contribution and can be easily fitted using and Aguado-Paniagua type expansion [19]. The quality of the above choice depends on how well the residual interaction will sum back to the total potential once added to the 2 body terms.

3.1 The (2B) contributions

The $V_{He_2}(R_j)$ potential was calculated again, for consistency with the rest of the PES, using CCSD(T) with aug-cc-pVQZ basis set. We computed 39 points from $r = 1.0$ to $12.0\,a_0$. The present results turned out to have only a 10% difference with the best potential available [20]. The analytic function for this system takes here the following form [19,21]: disregarding for the moment the much weaker dispersion contribution in He_2

$$V_{He_2}(R_j) = c_0 \frac{e^{-\alpha R_j}}{R_j} + \sum_{i=1}^{N} c_i \left(R_j e^{-\beta R_j}\right)^i \tag{6}$$

where c_0, c_i, α and β are determined by a non linear fitting procedure of our ab initio data. With $N = 9$ we obtained a RMS of 0.07 cm^{-1} and a maximum error of 0.14 cm^{-1}.

The fitting of $V_{He_2^+}(R_j)$ requires some modification of the form (6) because we have to include the much stronger long range polarizability interaction. We have therefore chosen the following analytic form

$$V(R_j) = V^{SR}(R_j)\,(1 - f(R_j)) + f(R_j)\,V^{LR}(R_j)$$

where the switching function [22] is

$$f(R_j) = \begin{cases} e\,\exp\left(-\dfrac{1}{1-x^n}\right), & x = \dfrac{R_c}{R_j} < 1, \\ 0 & x \geq 1. \end{cases} \tag{7}$$

The resulting function is finally given as

$$V_{He_2^+}(R_j) = f\left[c_0 \frac{e^{-\alpha R_j}}{R_j} + \sum_{i=1}^{N} c_i \left(r e^{-\beta R_j}\right)^i\right] - \frac{\alpha_{pol}}{2R_j^4}(1 - f(R_j)) \tag{8}$$

Table 1. Two-body parameters for $V_{He_2^+}(R_j)$ (Eq. (8)).

i	c_i
0	0.109871314(+02)
1	−0.398856858(+01)
2	0.948815040(+02)
3	−0.538670400(+04)
4	0.167824299(+06)
5	−0.321751784(+07)
6	0.370378724(+08)
7	−0.226612231(+09)
8	0.237177050(+09)
9	0.601725313(+10)
10	−0.318834945(+11)
12	0.814085212(+12)
13	−0.276188913(+13)
14	0.316397030(+13)
$\alpha_{He_2^+}$	1.6
$\beta_{He_2^+}$	1.59848334

where the helium polarizability value, α_{pol}, is given in the previous section. Using $N = 14$, with optimized switching parameters $R_c = 5.00973682\,a_0$ and $n = 3$, we have obtained deviations from the ab initio points inside the energy range of -30 cm^{-1} $< \Delta E <$ 19 cm^{-1} with relative errors of about 0.1%. Parameters for this He_2^+ fit are reported in Table 1; our computed parameters for the neutral interaction are not reported here, because it is possible to use those given in reference [20].

3.2 The (3B) contributions

The evaluation of this contribution is made after subtracting from the ab initio triatomic points the above fitted 2B terms, according to equation (4). We used about 3,232 points of the entire pool of ab initio values excluding the most repulsive geometries, i.e. those whose energy lies above the 3-atom break-up asymptote. The functional form of the 3-body contribution is:

$$V^{(3B)}(R_1, R_2, R_3) = \sum_{i,j,k}^{M} d_{ijk} F^{ijk}(\rho_1, \rho_2, \rho_3) \qquad (9)$$

where the coefficients were included under the following conditions:

$$\begin{aligned} &i + j + k \neq i \neq j \neq k \\ &i + j + k \leq M \\ &i \geq j \geq k \end{aligned}$$

and the function $F^{ijk}(\rho_1, \rho_2, \rho_3)$ keeps into account the correct symmetrization when needed

$$F^{ijk}(\rho_1\rho_2\rho_3) = \begin{cases} \rho_1^i\rho_2^j\rho_3^k, & i = j = k \\ \rho_1^i\rho_2^j\rho_3^k + \rho_1^j\rho_2^k\rho_3^i + \rho_1^k\rho_2^i\rho_3^j, & i = j > k \text{ or } i > j = k \\ \rho_1^i\rho_2^j\rho_3^k + \rho_1^j\rho_2^k\rho_3^i + \rho_1^k\rho_2^i\rho_3^j & \\ +\rho_1^i\rho_2^k\rho_3^j + \rho_1^j\rho_2^i\rho_3^k + \rho_1^k\rho_2^j\rho_3^i, & i > j > k \end{cases}$$

$\rho_n = R_n e^{-\beta^{(3)} R_n}$, $n = 1, 2, 3$.

where the last condition is a consequence of the high symmetry of the system. $\beta^{(3)}$ is the only nonlinear coefficient. In equation (9) no long-range part is present because all the long range terms have been already included in the 2B terms. Using $M = 14$ (132 linear terms), we found an optimized value of $\beta^{(3)} = 0.990436489$ and a standard deviation of 0.5644954 mHa. The most relevant deviations lie in the C_{2v} configurations, perhaps because of the anomalous shape of these curves due to the non-adiabatic interaction between two states. All the linear terms are reported in Table 2.

3.3 Results

Using the full functional form obtained by summing all the above contributions according to equation (4), we have therefore plotted different parts of the full 3D surface in Figure 5, where we can see some of the computed cuts. As shown at the center of the figure, the coordinates are r_1 and r_2, while the angle now is the one centered on the atom indicated in the figure; the zero of the energy is the full 3-atom break-up electronic energy. We can see that the plots are very smooth in all the regions explored, without any unrealistic oscillation. Furthermore, on each of the plots a minimum energy reaction pathway (MEP) has been shown. For the collinear approach geometry the system experiences a lowering of the energy in the symmetric configuration ($r_1 = r_2$) due to the vicinity of the triatomic minimum, while for smaller angles the pathway goes through a barrier.

This aspect is better described in Figure 6, where we compare the different MEP's of the previous figure using different arrangements.

In Figure 7 we present the energy along the bisector of the quadrant ($r_1 = r_2$ direction). The curve labelled "$He_2^+(r)$" that corresponds to a surface cut parallel to the r_2 axis for large r_1 values, is put as an eye-guiding comparison term between the "transition state" energy and the asymptotic one: the minimum in the collinear configuration corresponds to the global minimum of the triatomic system. It occurs, as we had already found in [1], in a linear symmetric configuration for $r_1 = r_2 = 2.34\,a_0$, with $E_0 = -2.645$ eV, while the minimum of the diatomic system to the asymptotic configuration lies at -2.466 eV.

In order to evaluate the errors in the more sensitive region of our fitting, we also plot a special cut of the

Table 2. Three-body linear parameters for $V^{(3B)}(R_1, R_2, R_3)$ (Eq. (9)).

i,j,k	d_{ijk}	i,j,k	d_{ijk}	i,j,k	d_{ijk}
1 1 0	−0.116357354(+01)	4 4 2	−0.284751563(+10)	11 1 0	0.105745708(+10)
1 1 1	0.264626472(+03)	5 3 2	0.695301644(+10)	5 4 4	0.103184726(+12)
2 1 0	0.730200921(+02)	5 4 1	0.187209641(+10)	5 5 3	−0.591686529(+12)
2 1 1	−0.966635761(+04)	5 5 0	0.118482508(+10)	6 4 3	0.247547154(+12)
2 2 0	0.250018521(+04)	6 2 2	−0.203137078(+10)	6 5 2	0.225930327(+12)
3 1 0	−0.183784890(+04)	6 3 1	−0.114572829(+10)	6 6 1	−0.188448192(+12)
2 2 1	0.965335702(+05)	6 4 0	0.571846341(+09)	7 3 3	−0.190654308(+12)
3 1 1	0.216579706(+06)	7 2 1	−0.951829960(+09)	7 4 2	−0.346644817(+12)
3 2 0	−0.362008810(+05)	7 3 0	0.343647915(+08)	7 5 1	0.589397180(+11)
4 1 0	0.150917204(+05)	8 1 1	0.852206371(+07)	7 6 0	0.101495564(+11)
2 2 2	−0.277401097(+07)	8 2 0	0.363418166(+08)	8 3 2	0.134911347(+12)
3 2 1	−0.608420665(+06)	9 1 0	0.220077043(+09)	8 4 1	0.684144595(+11)
3 3 0	0.870828468(+06)	4 4 3	−0.184413355(+11)	8 5 0	−0.224926137(+11)
4 1 1	−0.291699704(+07)	5 3 3	0.168362728(+11)	9 2 2	−0.611560568(+09)
4 2 0	0.153371073(+06)	5 4 2	0.353502438(+10)	9 3 1	−0.578602069(+11)
5 1 0	0.286179362(+05)	5 5 1	−0.167383595(+11)	9 4 0	0.722272752(+10)
3 2 2	0.124105283(+08)	6 3 2	−0.378657168(+11)	10 2 1	0.645380406(+10)
3 3 1	−0.702028346(+07)	6 4 1	0.580276547(+10)	10 3 0	0.862457219(+09)
4 2 1	0.840412475(+07)	6 5 0	−0.217293779(+10)	11 1 1	−0.114504405(+11)
4 3 0	−0.623522312(+07)	7 2 2	0.286957079(+11)	11 2 0	0.352759095(+10)
5 1 1	0.225991106(+08)	7 3 1	0.356682554(+10)	12 1 0	−0.938481424(+09)
5 2 0	−0.772716806(+06)	7 4 0	−0.151951980(+10)	5 5 4	−0.883552006(+12)
6 1 0	−0.134181683(+07)	8 2 1	−0.316434175(+10)	6 4 4	0.139364761(+13)
3 3 2	−0.101041716(+09)	8 3 0	0.296265511(+09)	6 5 3	0.371630684(+12)
4 2 2	0.101216889(+09)	9 1 1	−0.100506532(+10)	6 6 2	−0.533879090(+12)
4 3 1	0.647088389(+08)	9 2 0	0.637462755(+09)	7 4 3	−0.969248415(+12)
4 4 0	0.630884473(+08)	10 1 0	−0.607983303(+09)	7 5 2	0.211559996(+12)
5 2 1	−0.107629912(+09)	4 4 4	−0.157323898(+12)	7 6 1	0.122637126(+12)
5 3 0	0.177645370(+08)	5 4 3	0.870599145(+11)	7 7 0	−0.128862839(+11)
6 1 1	−0.954653281(+08)	5 5 2	−0.153450278(+12)	8 3 3	0.851955650(+12)
6 2 0	0.102932666(+08)	6 3 3	−0.876562746(+11)	8 4 2	0.315904623(+12)
7 1 0	0.112310935(+08)	6 4 2	0.939785399(+11)	8 5 1	−0.168659408(+12)
3 3 3	0.404299731(+09)	6 5 1	0.384235640(+11)	8 6 0	−0.389321203(+10)
4 3 2	−0.199055950(+09)	6 6 0	−0.325528284(+10)	9 3 2	−0.360288334(+12)
4 4 1	−0.554757373(+09)	7 3 2	0.573977420(+11)	9 4 1	0.173117265(+11)
5 2 2	−0.734148196(+09)	7 4 1	−0.497901521(+11)	9 5 0	0.264681926(+11)
5 3 1	−0.109400378(+09)	7 5 0	0.670665628(+10)	10 2 2	0.144482059(+12)
5 4 0	−0.259384119(+09)	8 2 2	−0.734326568(+11)	10 3 1	0.589652124(+11)
6 2 1	0.608213596(+09)	8 3 1	0.118964730(+11)	10 4 0	−0.179384235(+11)
6 3 0	−0.234607776(+08)	8 4 0	0.216607489(+10)	11 2 1	−0.276805777(+11)
7 1 1	0.186199180(+09)	9 2 1	0.953005999(+10)	11 3 0	0.339833885(+10)
7 2 0	−0.557080686(+08)	9 3 0	−0.169179065(+10)	12 1 1	0.121661074(+11)
8 1 0	−0.576837443(+08)	10 1 1	0.432784826(+10)	12 2 0	−0.215589008(+10)
4 3 3	−0.510322628(+08)	10 2 0	−0.236785034(+10)	13 1 0	0.263255752(+09)

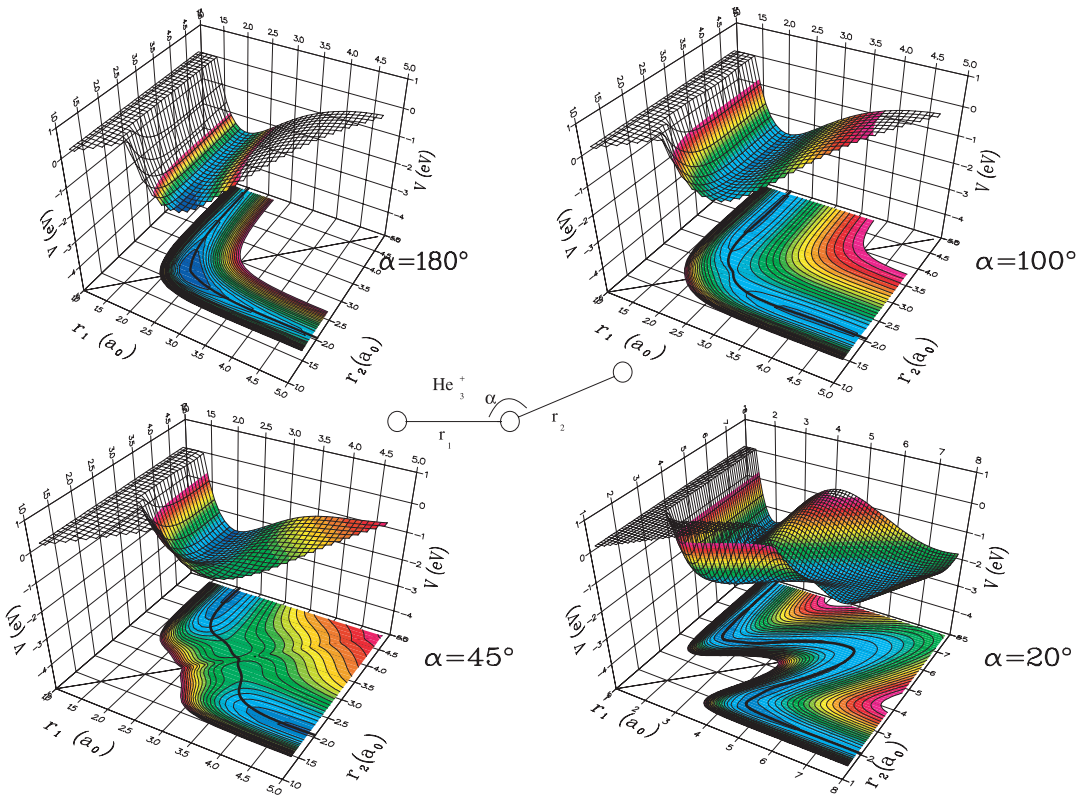

Fig. 5. Fitted PES cuts along different approaching geometries and their minimum energy paths.

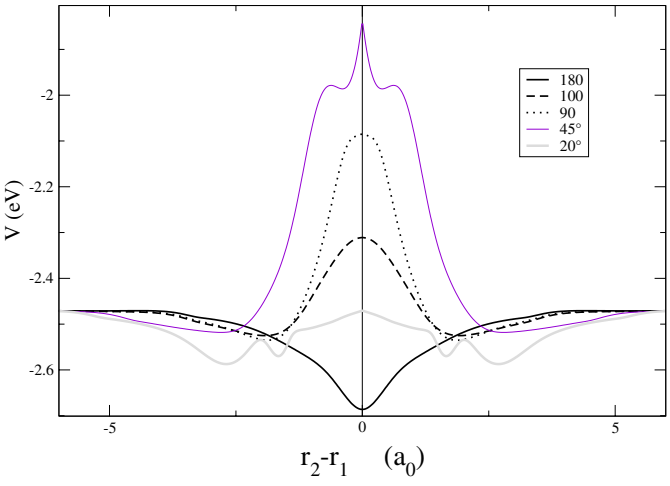

Fig. 6. Potential and corresponding r_1, r_2 values along the minimum energy path.

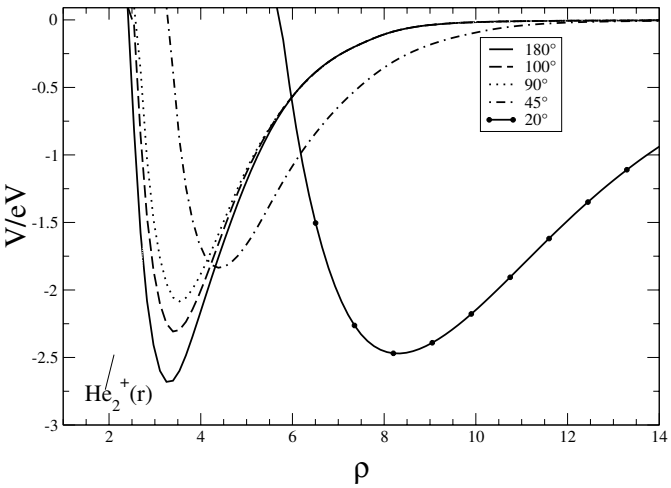

Fig. 7. Fitted surface cuts along the quadrant bisector, i.e. along the direction $r_1 = r_2$, with $\rho = (r_1^2 + r_2^2)^{1/2}$. The He_2^+ curve represents the two asymptotic channels ($r_1 \gg r_2$ or the opposite) and is put there for an visual comparison with the present data ($r_1 = K$, with $K > 10\,a_0$, or the opposite).

surface in the C_{2v} configuration, switching back to the Jacobi coordinates. The resulting contour plots are shown in Figure 8 where the discontinuity due to the presence of the higher electronic state is clearly seen and occurs when the system goes through the D_{3h} geometry, i.e. when $R_1 = R_2 = R_3$. The C_{2v} surface is also useful for a comparison with the only existing fit for this system as given by reference [15], where the authors employed a very accurate MRCI procedure over a small set of points around the C_{2v} configuration. At this point it is worth noticing that our CCSD(T) approach has some obvious limitations for the present system, because it lacks a multideterminantal initial guess for calculations around the surface regions where different states intersect (C_{2v}). We have already discussed this problem in a previous paper [23]. In the present case the strength of the interaction turns out to be quite small outside a very narrow cone near the crossing seam and our calculations describe this feature fairly realistically, as one can gather by comparing our Figure 8

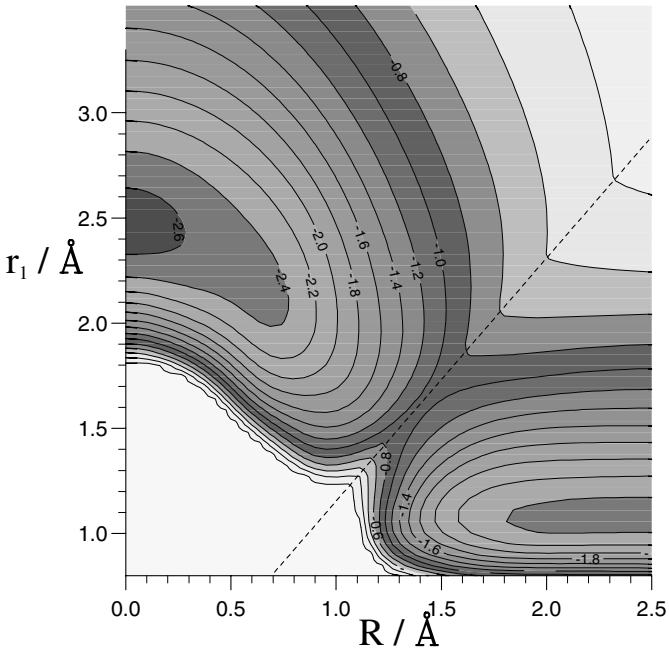

Fig. 8. Isoenergetic contours of the potential in C_{2v} configuration. The dashed line defines the D_{3h} symmetry situation for the complex and the corresponding seam between the $^2A_1$ and $^2B_1$ electronic states.

with the same figure (Fig. 1) of reference [15], where the two separate electronic states ($^2A_1$ and $^2B_1$) are reported. Such a comparison is shown more quantitatively in Table 3, where our fitted points are reported and compared with the lower energy adiabatic curve calculated in [15], together with the difference values ΔV.

Table 3. A comparison between the results from our analytical fitting (V_{fit}) and the ab initio energies computed by Knowles et al. [15] in the C_{2v} geometry (V_{KM}, the lower-lying value between the two computed curves is reported). Distances in Å, energies in eV.

R_1	R_2, R_3	V_{KM}	V_{fit}	ΔV
0.8	1.4	−0.24085	−0.10113	0.13972
1.0	1.3	−0.85326	−0.69383	0.15943
1.2	1.2	0.54792	0.38542	−0.16250
1.4	1.1	−0.82711	−0.84767	−0.02056
1.6	1.0	−0.98164	−1.00184	−0.02020
0.8	2.0	−0.97661	−0.92258	0.05403
1.0	1.9	−2.38498	−2.34819	0.03679
1.2	1.8	−2.26027	−2.20583	0.05444
1.4	1.7	−1.64225	−1.51908	0.12317
1.6	1.6	−0.88850	−0.92234	−0.03384
1.8	1.5	−1.56543	−1.58321	−0.01778
2.0	1.4	−2.07621	−2.05456	0.02165
2.2	1.3	−2.44520	−2.46054	−0.01534
2.4	1.2	−2.63230	−2.66504	−0.03274
1.0	2.5	−2.42142	−2.38657	0.03485
1.2	2.4	−2.38702	−2.35191	0.03511
1.4	2.3	−1.92068	−1.88131	0.03937
1.6	2.2	−1.40930	−1.35286	0.05644
1.8	2.1	−0.97179	−0.88651	0.08528
2.0	2.0	−0.62414	−0.63772	−0.01358
2.2	1.9	−0.92466	−0.94351	−0.01885
2.4	1.8	−1.21942	−1.21453	0.00489
2.6	1.7	−1.52119	−1.51087	0.01032

4 The rotovibration-to-translation coupling potential

The first step in the study of the quantum dynamics of the title system requires the evaluation of the coupling potentials between the rotovibrational degrees of freedom of the dimer ion and the relative translational motion, the (R,V-T) coupling potential:

$$\langle \varphi_i(r)| \, V(r, R, \theta) \, |\varphi_j(r)\rangle = V_{ij}(R, \theta) \qquad (10)$$

where (r, R, θ) are the Jacobi coordinates which describe the internal vibrational diatomic motion (r), the atom-diatomic distance (R) and their relative orientation angle, θ. The physical meaning of these matrix elements is fairly evident: the diagonal terms represent the asymptotic (diabatic) averaging of the full PES over each vibrational target state, implicitly assuming that such state does not change much during the collisional interaction. On the other hand the off diagonal terms describe the effects by which the triatomic potential couples different asymptotic states of the diatomic system during the scattering process, thereby allowing transitions between them due to the impinging projectile, and thus describing the deformations of the vibrating ionic dimer due to its interaction with the impinging projectile.

The analysis of the vibrational coupling strength for each V_{ij} term is crucial for evaluating the relative efficiency of the energy transfer dynamics between any two (i, j) vibrational target states. This aspect of the problem, in fact, will be analysed in detail (via the present interaction) in a following paper [13]. In our calculations we considered all the bound vibrational levels, for which the integrals of equation (10) are found to have converged within the radial region mapped by the triatomic ab initio potential: it allowed us to include up to $\nu_{max} = 19$. Looking at the strength of such terms at different radial distances and orientations allow us to estimate the likely efficiency of the collision dynamics. We further employed the previous 3D fitting to generate the corresponding coupling elements up to the top bound state of He_2^+ ($\nu = 23$). We show in Figure 9 a sampling of their behaviour for different vibrational levels. In the upper panel a cut at $\theta = 0$ for some of the $\Delta\nu = 1$ matrix elements in their attractive region is shown and is compared with their corresponding diagonal elements that give us the elastic channel couplings described above. We clearly see that the potential wells are invariably strong, never less than 1000 cm^{-1}, even when the energy spacings between the levels become

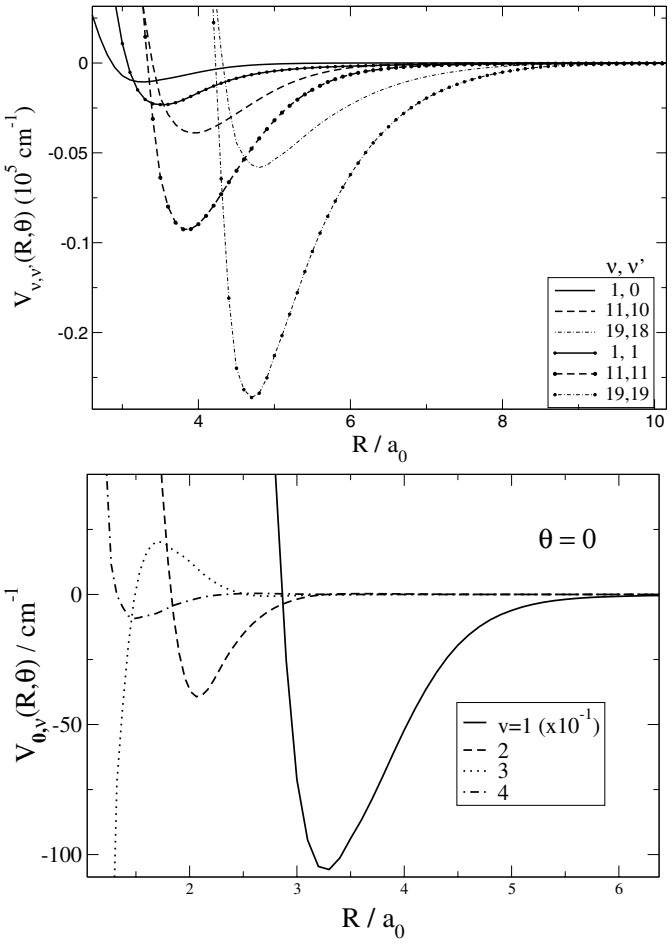

Fig. 9. Vibrational coupling potentials for the $He_2^+ + He$ interaction in the linear configuration ($\theta = 0$). Single quantum transitions ($\Delta\nu = 1$, upper panel) from different initial levels compared with the corresponding elastic channel and multiple quantum transitions from the ground state (lower panel). In the latter the first element is scaled by a factor of 10.

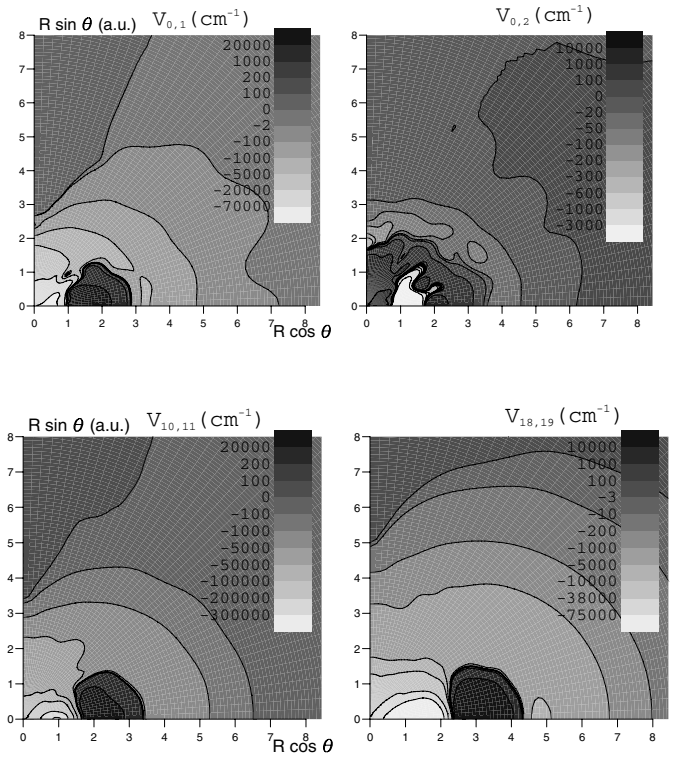

Fig. 10. $He_2^+ - He$ Vibrational Coupling PES in Cartesian coordinates: some selected matrix elements.

very large (for levels far apart on the vibrational ladder) and that the off-diagonal matrix elements are always comparable in size to the diagonal ones. The lower panel of the same figure shows a cut at $\theta = 0$ through the couplings for transitions with $\Delta\nu > 1$: it is evident the large difference in magnitude between them (the single quantum term in the figure is scaled by a factor of 10), but it is also useful to note that the couplings do not go to zero even when $\Delta\nu = 4$. This is a useful piece of information because it leads us to think that relaxations to the lower levels would still be contributing for multiple step processes, and thus the overall relaxation process could be made faster because of them. One should also keep in mind that the present potential also naturally includes coupling of the dimer rotational motion with the impinging He motion via the angular anisotropy of the full surface. We have already discussed this aspect of the coupling in [1] and will also further analyse it in [13].

In Figure 10 we show contour maps in Cartesian coordinates of the orientational behaviour of some of the matrix elements of our coupling potential. The limits of the Jacobi representation discussed before is the cause of some spurious oscillations introduced by the visualization software. However, one can clearly see that the single quantum transitions are always behaving smoothly and maintain their strength over a fairly broad angular range, although the maxima invariably appear in the collinear configuration. The angular regions of the surface close to the C_{2v} geometry show in fact a fairly small coupling strength up to relatively short radial distances (around $4\,a_0$). This could be understood when considering that an He atom coming along this approach causes negligible perturbation of the target ion unless it strikes it exactly at its center of mass. On the other hand, in the collinear region the interaction is always strong, as is within the angular cone close to it, where the interaction is driven by the exchange, short range, interaction terms. The shape of the inelastic coupling surface for the V_{02} matrix element is shown in the upper right panel of Figure 10. It is more complicated in shape than the previous coupling element and the preferred approaching geometry is now that of 90°, where the coupling strength is even larger than that for the single quantum coupling surfaces discussed before. We can again suggest that at any relative orientation of approach some vibrational coupling that connects a given level with the next one, or with a more distant one in the sequential ladder of the target asymptotic vibrational states, seems

always to be present. The orientational dependence of the coupling terms also tells us that rotational and vibrational couplings are closely entangled in the present system and will inevitably play a common role in the dynamics, as we shall be discussing in the following paper [13].

5 Present conclusions

A new, accurate Potential Energy Surface has been computed for the system He_3^+ using CCSD(T) on a very dense spatial grid. An accurate three-body fitting procedure has been carried out obtaining a well-behaving analytic description of the full interaction that can be employed for dynamical studies involving rearrangement collisions. The coefficients file, as well as the subroutine generating the potential, are also available on request from the authors. The (R,V-T) coupling potential has also been computed involving all the bound vibrational states of the ionic dimer over a broad angular range of the triatomic potential, and the resulting values reveal very large coupling strength among most of them, with a dominance of single quantum jumps but also with considerable strength being allotted to larger $\Delta\nu$ matrix elements. This is indeed an indication of the likely efficiency of the collisional relaxation mechanism from an excited He_2^+ interacting with surrounding neutral He atoms in large helium clusters, as we shall analyse later [13]. In our following work (part III [13]) we will thus focus in greater detail on the evaluation of that process cross sections by modelling the collisions and the cooling rates. Such a study will allow to understand more quantitatively the relative time scales of the post-ionization dynamics.

We are grateful to Dr. Rocco Martinazzo for his help in the choice and use of the fitting procedure and to Prof. Miguel Paniagua for helping us with the use of *GFIT3C*. The financial support of the CASPUR Supercomputing Center, the Scientific Research Committee of the University of Rome "La Sapienza" and of the INFM is also gratefully acknowledged.

References

1. E. Scifoni, F.A. Gianturco, Eur. Phys. J. D **21**, 323 (2002)
2. *Clusters of atoms and molecules,* edited by H. Haberland (Springer-Verlag, Berlin Heidelberg, 1994)
3. *Cluster Ions*, edited by C.Y. Ng, T. Baer, I. Powis (Wiley, New York, 1993)
4. P.J. Knowles, J.N. Murrell, Mol. Phys. **87**, 827 (1996)
5. B.E. Callicoatt, K. Förde, L.F. Jung, T. Ruchti, K.C. Janda, J. Chem. Phys. **109**, 10195 (1998)
6. M. Ovchinnikov, B.L. Grigorenko, K.C. Janda, V.A. Apkarian, J. Chem. Phys. **108**, 9351 (1998)
7. F. Filippone, F.A. Gianturco, Europhys. Lett. **44**, 585 (1998)
8. V. Ariyente, I. Baccarelli, B. Balta, F.A. Gianturco, C. Selçuki, in *Quantum Systems in Physics and Chemistry*, edited by R.M. Weeny, R. Wilson (Kluwer Academic Publishers, 1998)
9. J.P. Toennies, A.F. Vilesov, Annu. Rev. Phys. Chem. **49**, 1 (1998)
10. K.K. Lehmann, Mol. Phys. **97**, 645 (1999)
11. B. Balta, F.A. Gianturco, F. Paesani, Chem. Phys. **254**, 215 (2000)
12. F. Stienkemeier, A. Vilesov, J. Chem. Phys. **115**, 10119 (2001)
13. E. Scifoni, E. Bodo, G. Dellepiane, F.A. Gianturco, Eur. Phys. J. D **30**, 363 (2004)
14. M.F. Satterwhite, G.I. Gellene, J. Chem. Phys. **99**, 13397 (1995)
15. P.J. Knowles, J.N. Murrell, E.J. Hodge, Mol. Phys. **85**, 243 (1995)
16. E. Bodo, E. Scifoni, F. Sebastianelli, F.A. Gianturco, A. Dalgarno, Phys. Rev. Lett. **89**, 283201 (2002)
17. M.J. Frisch, G. Trucks, H. Schlegel, P.M.W. Fill, B.G. Johnson, M.A. Robb, J.R. Cheeseman, T.A. Keith, G.A. Petersson, J.A. Montgomery, et al., *GAUSSIAN 94 (revision D.1)*, Gaussian inc., pittsburgh pa ed. (1995)
18. U. Hohm, Mol. Phys. **69**, 803 (1990)
19. A. Aguado, M. Paniagua, J. Chem. Phys. **96**, 1265 (1992)
20. R.A. Aziz, F.R.W. McCourt, C.C.K. Wong, Mol. Phys. **61**, 1487 (1987)
21. A. Aguado, C. Tablero, M. Paniagua, Comp. Phys. Comm. **108**, 259 (1998)
22. R. Martinazzo, G.F. Tantardini, E. Bodo, F.A. Gianturco, J. Chem. Phys. **119**, 11241 (2003)
23. F.A. Gianturco, M.P. de Lara-Castells, F. Schneider, J. Chem. Phys. **107**, 1522 (1997)